Electronic Supplementary Material (ESI) for Journal of Materials Chemistry A.


# Nanocrystalline $CoO_x$ Glass for Highly-efficient Alkaline Hydrogen Evolution Reaction

Jinxian Feng [a], Lulu Qiao [a], Pengfei Zhou [a], Haoyun Bai [a], Chunfa Liu [a], Chon Chio Leong [b], Yu-Yun Chen [a], Weng Fai Ip [c], Jun Ni [d] and Hui Pan [ac] *

[a] *Institute of Applied Physics and Materials Engineering, University of Macau, Macao S. A. R., China*

[b] *Department of Electrical and Computer Engineering, Faculty of Science and Technology, University of Macau, Macao S. A. R., China*

[c] *Department of Physics and Chemistry, Faculty of Science and Technology, University of Macau, Macao S. A. R., China*

[d] *Institute of Industrial Catalysis, Zhejiang University of Technology, Hangzhou, 310014, China*

Hui Pan: huipan@um.edu.mo (email), +853-88224427 (tel.), +853-88222454 (fax).

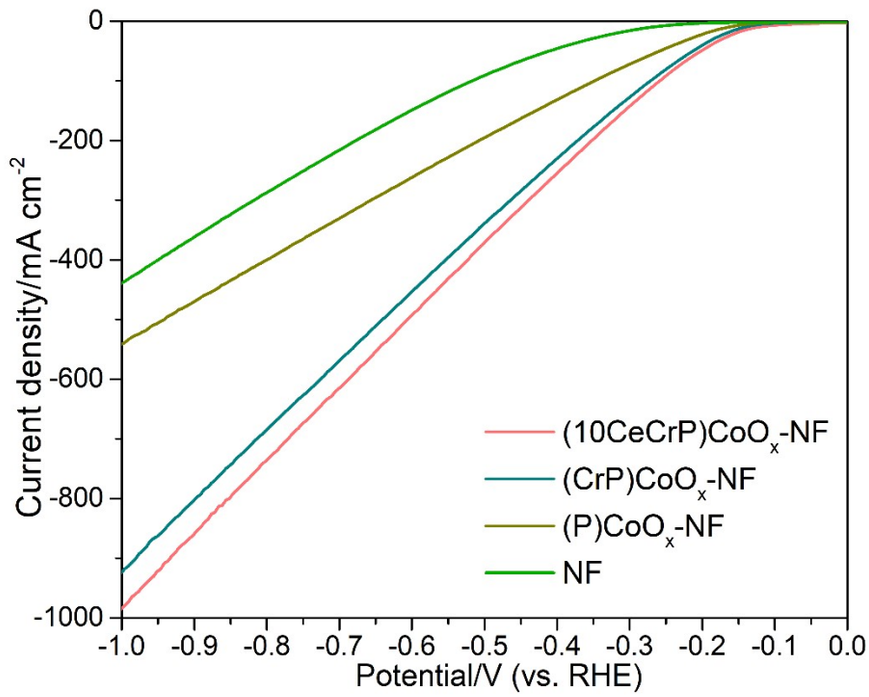


**Figure S1.** LSV curves of $(10CeCrP)CoO_x$-NF, $(CrP)CoO_x$-NF, $(P)CoO_x$-NF and NF.

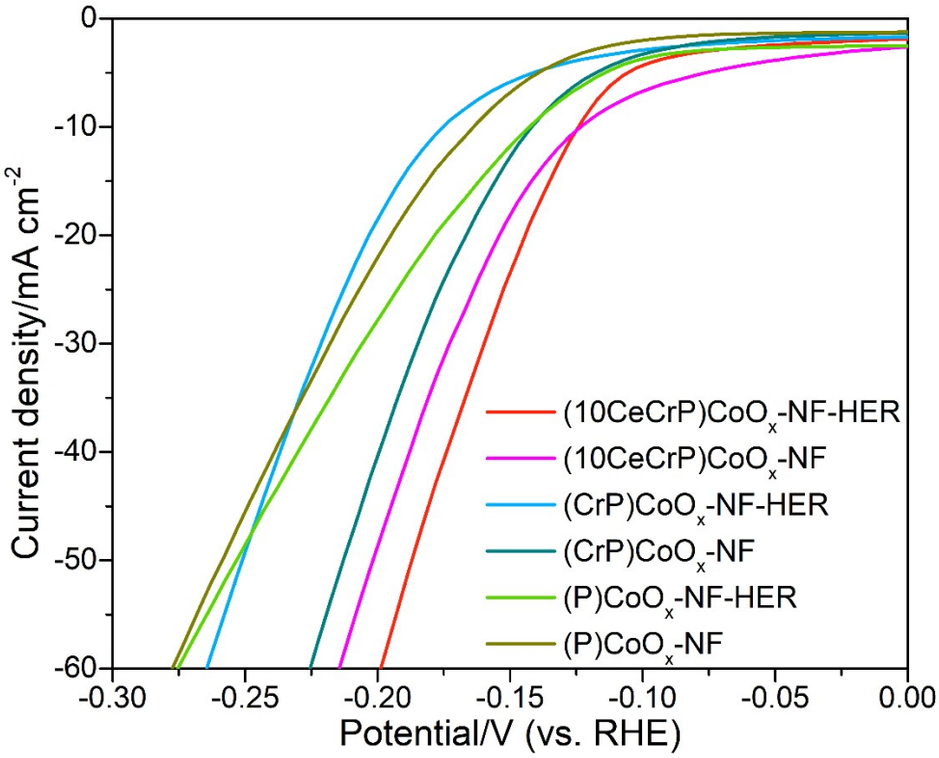


**Figure S2.** LSV curves of (10CeCrP)$CoO_x$-NF, (10CeCrP)$CoO_x$-NF-HER, (CrP)$CoO_x$-NF, (CrP)$CoO_x$-NF-HER, (P)$CoO_x$-NF and (P)$CoO_x$-NF-HER within 0 ~ -0.3 V.

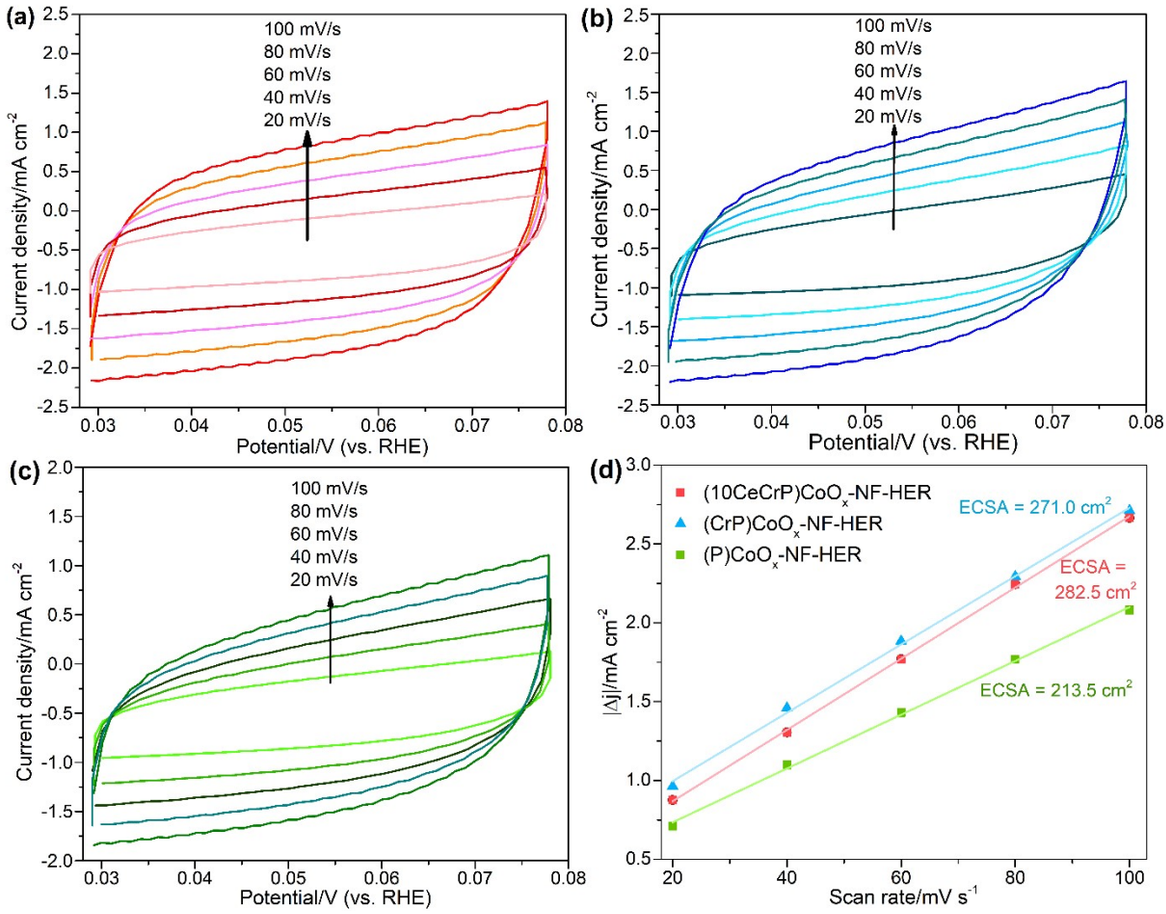


**Figure S3.** CV curves: (a) (10CeCrP)$CoO_x$-NF-HER, (b) (CrP)$CoO_x$-NF-HER and (c) (P)$CoO_x$-NF-HER with different scan rates. (d) ECSAs of (10CeCrP)$CoO_x$-NF-HER, (CrP)$CoO_x$-NF-HER and (P)$CoO_x$-NF-HER.

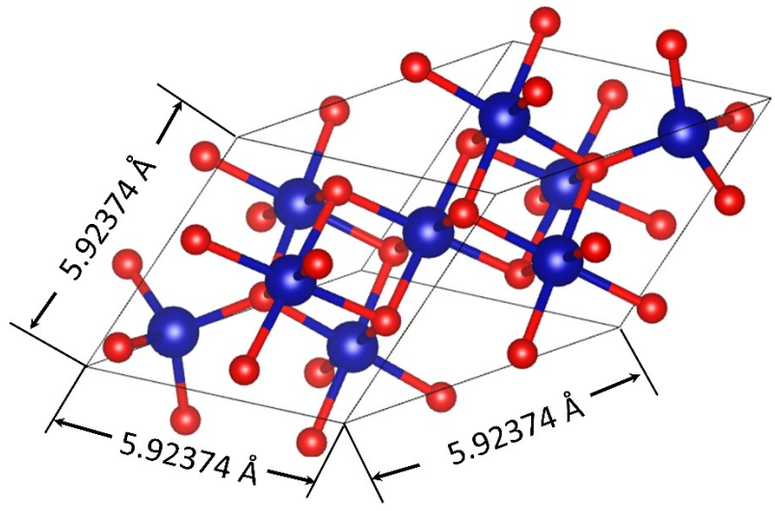


**Figure S4.** $Co_3O_4$ unit cell. Cell volume: 144.3 $Å^3$; total atoms: 14 (6Co + 8O) (Blue: Co, red: O).

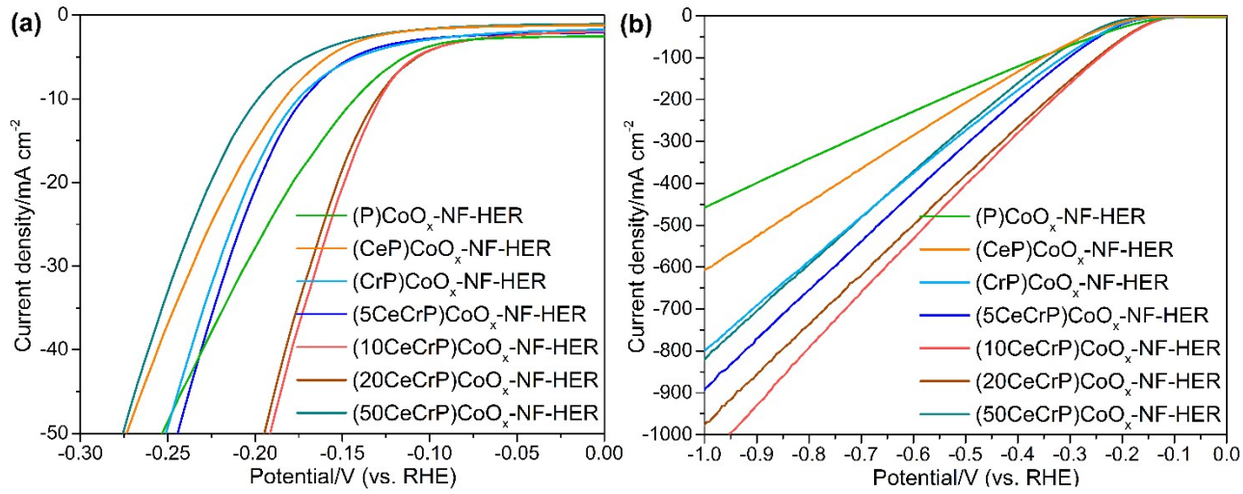


**Figure S5.** LSV curves of (P)$CoO_x$-NF-HER, (CeP)$CoO_x$-NF-HER, (CrP)$CoO_x$-NF-HER and (xCeCrP)$CoO_x$-NF-HER at different potential intervals: (a) 0 ~ -0.3 V and (b) 0 ~ -1.0 V.

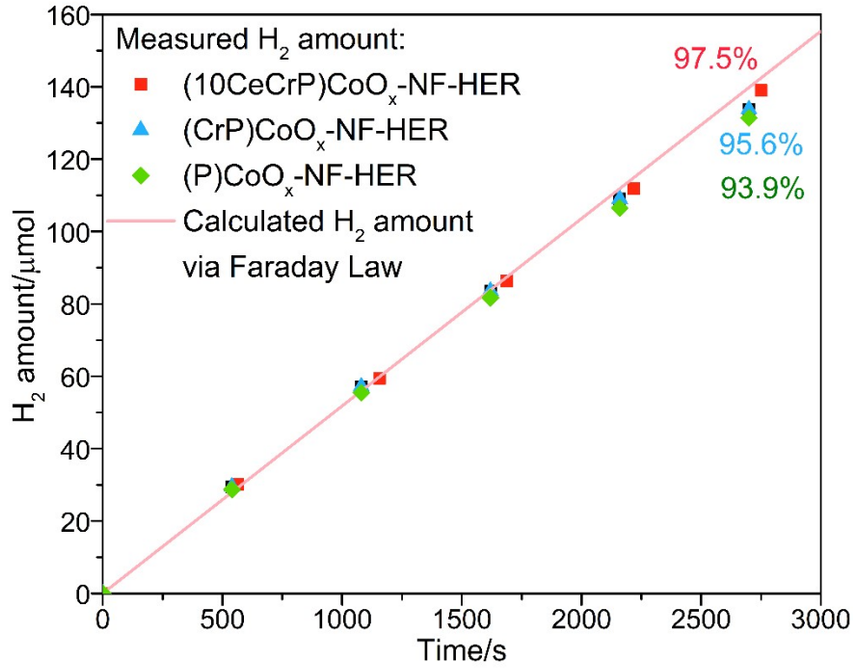


**Figure S6.** The theoretically calculated (red line) and experimentally measured (colored dots) hydrogen vs. time for (P)$CoO_x$-NF-HER, (CrP)$CoO_x$-NF-HER and (10CeCrP)$CoO_x$-NF-HER at 20 mA $cm^{-2}$.

**Table S1.** Comparison of (10CeCrP)$CoO_x$-NF-HER and other reported electrocatalysts with similar composition in 1 M KOH.

| Electrocatalyst | Loading mass/mg per $cm^2$ | Current density/mA $cm^{-2}$ (Potential/V vs. RHE) | iR-correction | Reference |
|---|---|---|---|---|
| (10CeCrP)$CoO_x$-NF-HER | 0.31 | 10 (-0.128)<br>50 (-0.193)<br>100 (-0.245)<br>200 (-0.354)<br>500 (-0.580) | No | This work |
| $CoFeO_x(OH)_y/CoO_x(OH)_y$ | 0.27 | 10 (-0.26)<br>50 (-0.32)<br>100 (-0.37) | Corrected | Electrochimica Acta 391 (2020) 136038 |
| Co-WC@G/ PCSs | 0.85 | 30 (-0.17)<br>100 (-0.2) | Corrected | ACS Appl. Nano Mater. 2021, 4, 11870−11880 |
| CoP@BCN | 0.4 | 10 (-0.210)<br>20 (-0.280) | No | Adv. Energy Mater. 2017, 1601671 |
| CoP@$CoO_x$ | 1.5 | 50 (-0.1)<br>100 (-0.109) | Corrected | ACS Appl. Energy Mater. 2020, 3, 309−318 |
| Ru/$Co_4N$-$CoF_2$ | 3.5 | 10 (-0.053)<br>50 (-0.175)<br>100 (-0.220) | 95% iR compensation | Chem. Eng. J. 414 (2021) 128865 |
| CoP@a-$CoO_x$ plate | 1.5 | 10 (-0.18)<br>100 (-0.25) | Corrected | Adv. Sci. 2018, 5, 1800514 |
| Co-CoO/$ZnFe_2O_4$@CNWs | 0.5 | 10 (-0.226)<br>20 (-0.30) | -- | J. Colloid and Interface Sci. 561 (2020) 620–628 |
| N-C-Co20-100Pd | 3.5 | 10 (-0.140)<br>50 (-0.150) | 95% iR compensation | J. Mater. Chem. A, 2021, 9, 17724–17739 |
| CoP/N-doped carbon | 0.42 | 10 (-0.167)<br>25 (-0.180) | No | Electrochimica Acta 375 (2021) 137966 |
| Co/$CoO_x$ | -- | 10 (-0.220) | No | Nano Energy 32 |

| | | | | |
|---|---|---|---|---|
| nanoshoots/perovskite | | 50 (-0.270)<br>100 (-0.30) | | (2017) 247–254 |
| NiCo-N<br>-O nanosheet hybrids | -- | 50 (-0.150)<br>100 (-0.190) | 90% iR compensation | Mater. Today Energy 21 (2021) 100784 |
| $CoO_x$-N-C/$TiO_2C$ | 0.283 | 10 (-0.38) | No | Journal of Power Sources 414 (2019) 333–344 |
| $V_{Zn}$-ZnCoPi-OH | 12 | 50 (-0.160)<br>100 (-0.180) | 95% iR compensation | Mater. Today Phys. 20 (2021) 100448 |
| $CoO_x$ catalyst in-situ grown on Co foam | --- | 20 (-0.112)<br>50 (-0.150)<br>100 (-0.190) | iR compensation | Front. Chem., 2020, 8, 386 |
| CoP/o-CC | 0.32 | 50 (-0.20)<br>100 (-0.23)<br>200 (-0.260) | Corrected | Inter. J. Hydrogen Energy. 2022 47 9209 |
| CoFe/$N_H$-C NS | 1.8 | 10 (-0.28)<br>50 (-0.350) | Corrected | ACS Sustainable Chem. Eng. 2019, 7, 15278−15288 |
| Co@C/NC | 0.4 | 10 (-0.175)<br>50 (-0.280)<br>100 (-0.370) | 80% iR compensation | Energy Fuels 2022, 36, 1688−1696 |
| Ni, S-Codoped CoO | 0.87 | 50 (-0.180)<br>100 (-0.225)<br>200 (-0.250) | Corrected | ACS Sustainable Chem. Eng. 2019, 7, 12501−12509 |
| CFC-CNT-$CoO_x$/CoP | 0.41 | 10 (-0.108)<br>50 (-0.152) | 90% iR compensation | Chem. Engineering J. 416 (2021) 128943 |
| $CoO_x$/$CoN_y$@CN | 0.283 | 10 (-0.320)<br>50 (-0.380)<br>80 (-0.410) | Corrected | Appl. Cat. B: Environ. (2020) 279 119407 |
| Co-$NiS_2$ NSs | 0.84 | 10 (-0.08)<br>50 (-0.160)<br>100 (-0.20) | Corrected | Angew. Chem. Int. Ed. 2019, 58, 18676 – 18682 |
| N-doped CoO nanowire arrays | -- | 10 (-0.123)<br>50 (-0.220) | -- | Catalysts 2021, 11, 1237 |

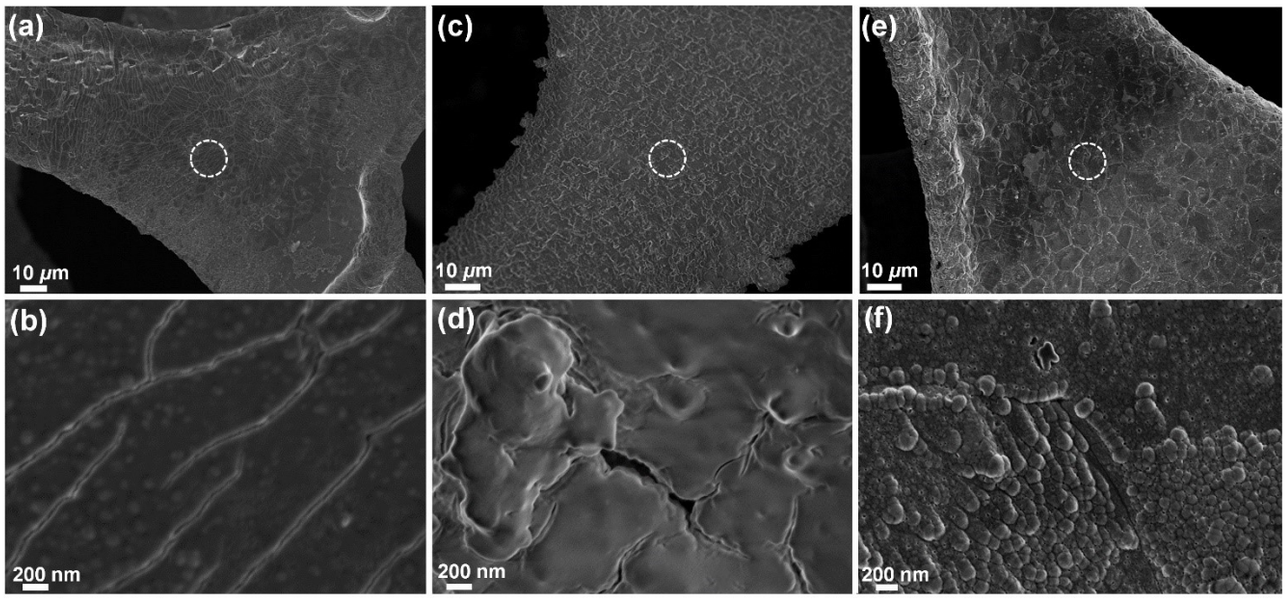


**Figure S7.** SEM images: (a-b) (10CeCrP)$CoO_x$-NF, (c-d) (CrP)$CoO_x$-NF, and (e-f) (P)$CoO_x$-NF.

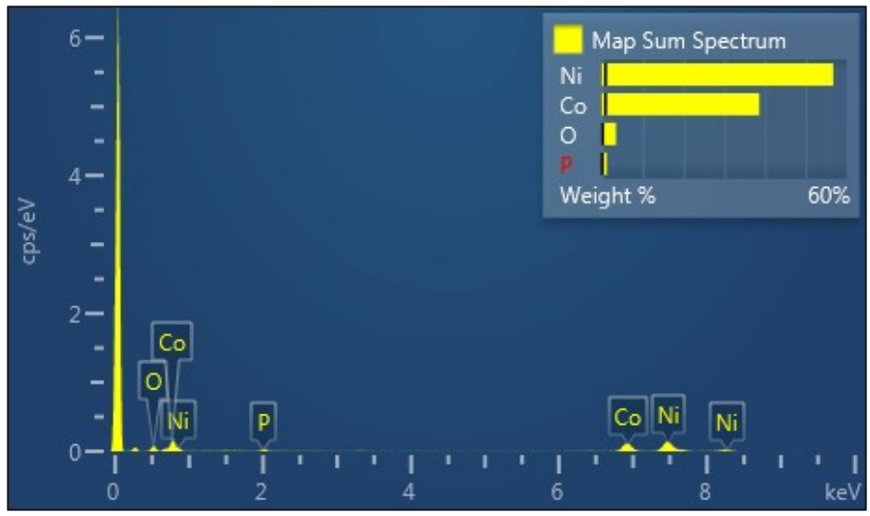


**Figure S8.** EDS spectrum of (P)$CoO_x$-NF-HER.

**Table S2.** Elemental composition of (P)$CoO_x$-NF-HER

| Element | Atomic % |
|---|---|
| O | 11.56 |
| P | 2.11 |
| Co | 34.89 |
| Ni | 51.45 |
| Total: | 100.00 |

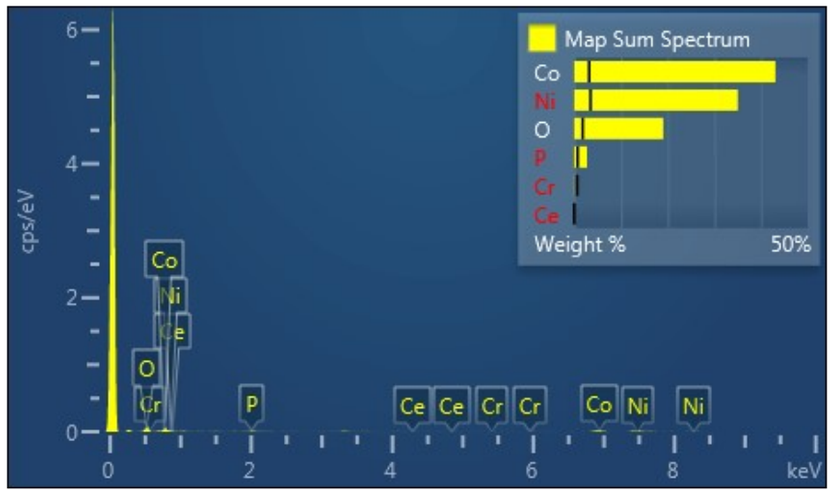


**Figure S9.** EDS spectrum of (CrP)$CoO_x$-NF-HER.

**Table S3.** Elemental composition of (CrP)$CoO_x$-NF-HER

| Element | Atomic % |
|---|---|
| O | 45.68 |
| P | 3.39 |
| Cr | 0.08 |
| Co | 28.00 |
| Ni | 22.84 |
| Ce | 0.00 |
| Total: | 100.00 |

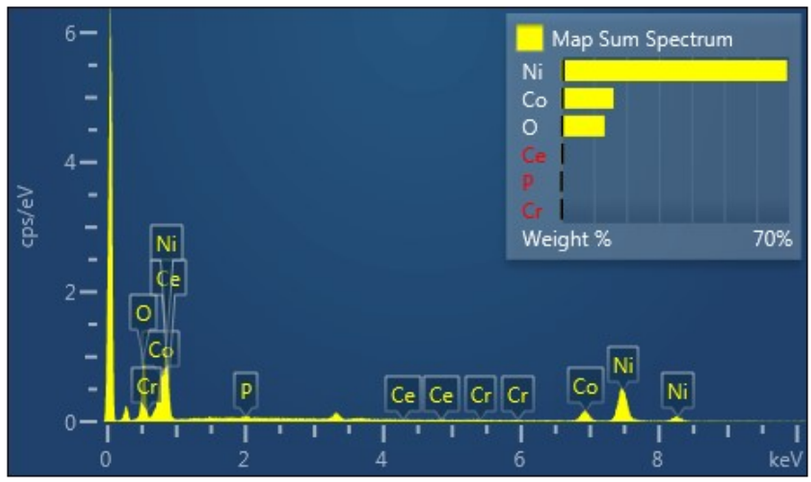


**Figure S10.** EDS spectrum of (10CeCrP)$CoO_x$-NF-HER.

**Table S4.** Elemental composition of (10CeCrP)$CoO_x$-NF-HER

| Element | Atomic/% |
|---|---|
| O | 36.15 |
| P | 0.59 |
| Cr | 0.12 |
| Co | 11.81 |
| Ni | 51.11 |
| Ce | 0.21 |
| Total: | 100.00 |

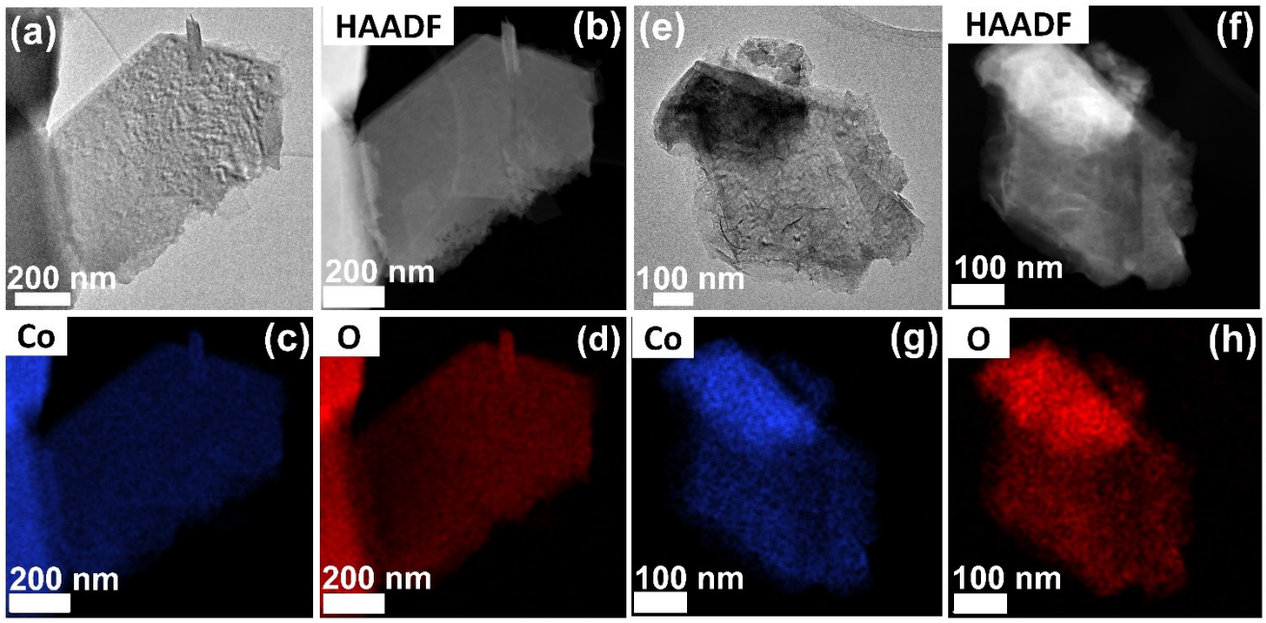


**Figure S11.** (CrP)$CoO_x$-NF-HER: (a) TEM image, (b) STEM-HAADF, and (c-d) EDS elemental mappings of Co and O. (P)$CoO_x$-NF-HER: (e) TEM image, (f) STEM-HAADF, and (g-h) EDS elemental mappings of Co and O.

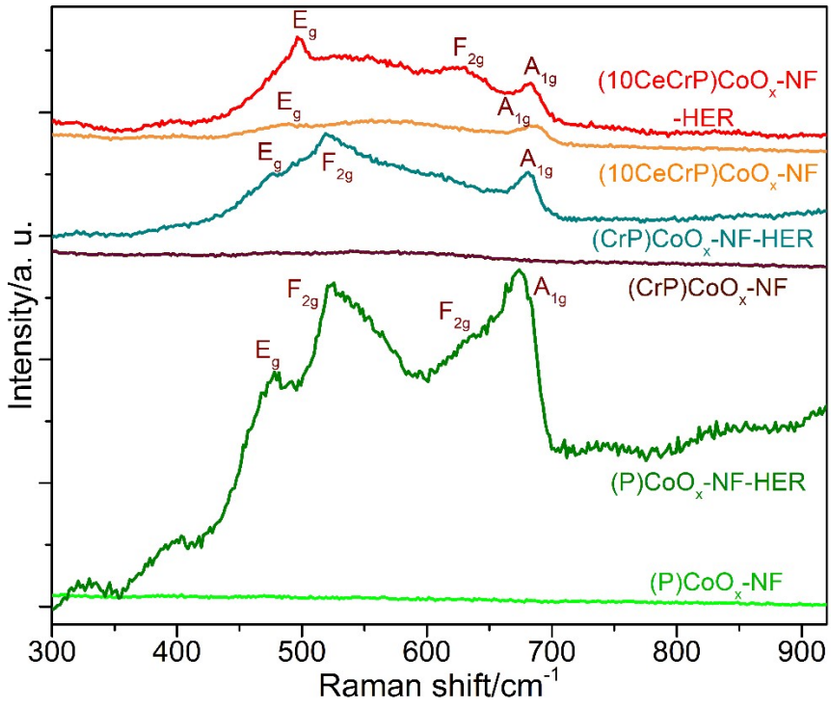


**Figure S12.** Raman spectra of (P)$CoO_x$-NF, (CrP)$CoO_x$-NF and (10CeCrP)$CoO_x$-NF before and after HER.

The Raman spectra (Figure S12) show that (CrP)$CoO_x$-NF and (P)$CoO_x$-NF-HER show negligible characteristic peak of $CoO_x$ However, the peaks are obvious after the HER test.[1, 2] Meanwhile, we can also see that the intensities of $CoO_x$ characteristic peaks of (10CeCrP)$CoO_x$-NF-HER are stronger than those of (10CeCrP)$CoO_x$-NF. Therefore, the crystallinity of $CoO_x$ was enhanced during HER.

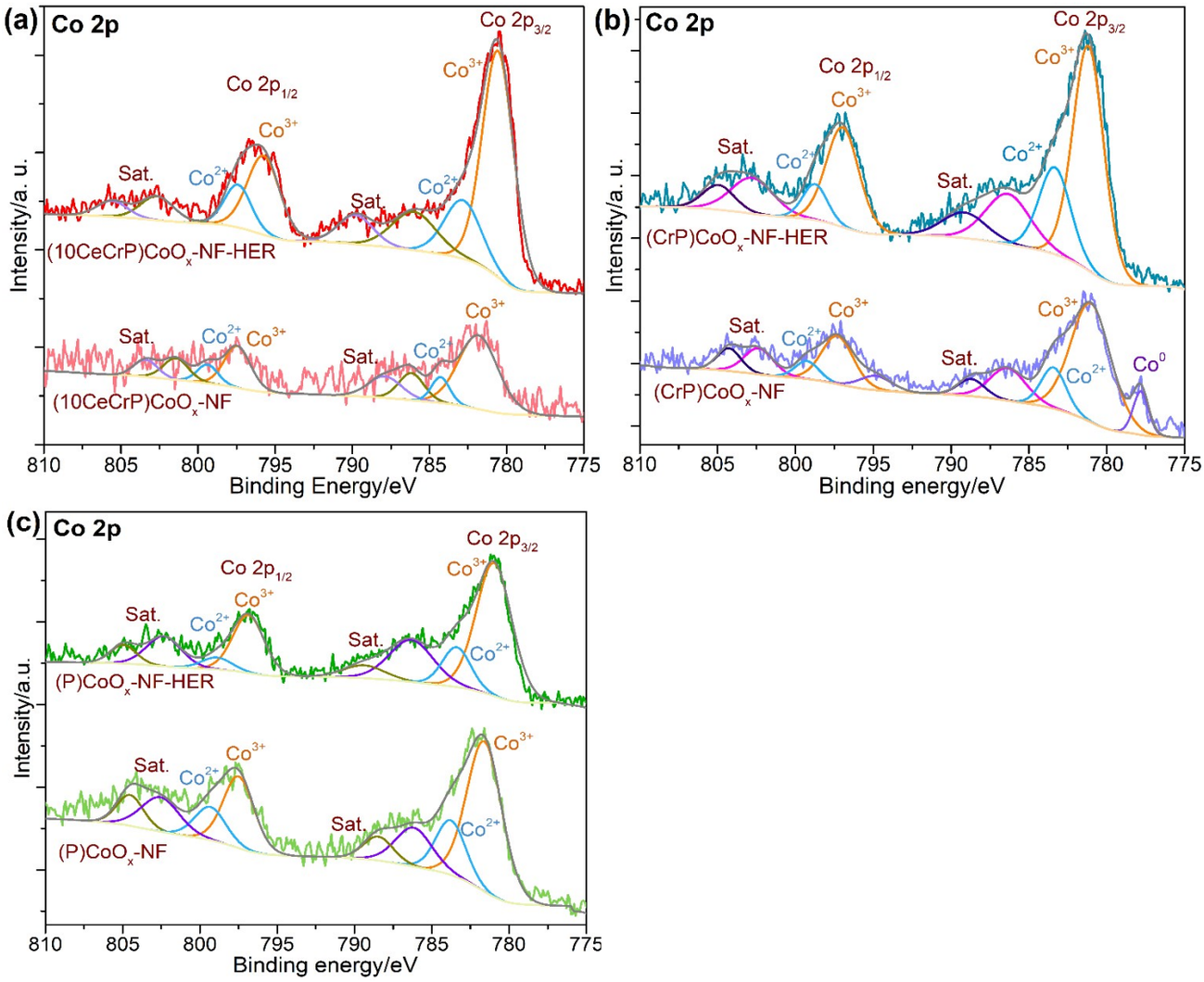


**Figure S13.** XPS spectra of (a) (10CeCrP)$CoO_x$-NF, (b) (CrP)$CoO_x$-NF and (c) (P)$CoO_x$-NF before and after HER.

The chemical states of Co in (P)$CoO_x$-NF, (CrP)$CoO_x$-NF and (10CeCrP)$CoO_x$-NF before and after HER were studied by XPS. The Co 2p XPS spectra of (10CeCrP)$CoO_x$-NF and (10CeCrP)$CoO_x$-NF-HER have eight main peaks, including Co $2p_{3/2}$ and $2p_{1/2}$ peaks for both $Co^{3+}$ and $Co^{2+}$ in $Co_3O_4$, as well as their satellite peaks (Figure S13a). The Co 2p spectrum of (CrP)$CoO_x$-NF-HER shows eight main peaks too. But the Co 2p spectrum of (CrP)$CoO_x$-NF shows ten main peaks, including Co $2p_{3/2}$ and $2p_{1/2}$ peaks for metallic Co ($Co^0$), and their satellite peaks (Figure S13b). For the Co 2p spectra of (P)$CoO_x$-NF and (P)$CoO_x$-NF-HER, eight main peaks for both $Co^{3+}$ and $Co^{2+}$ in $Co_3O_4$, as well as their satellite peaks can be seen (Figure S13c).[3-5] Comparing the Co 2p spectra of (P)$CoO_x$-NF, (CrP)$CoO_x$-NF and (10CeCrP)$CoO_x$-NF before and after HER, the peak intensities and areas of different Co characteristic signals change, suggesting the chemical states of Co change during the HER process.

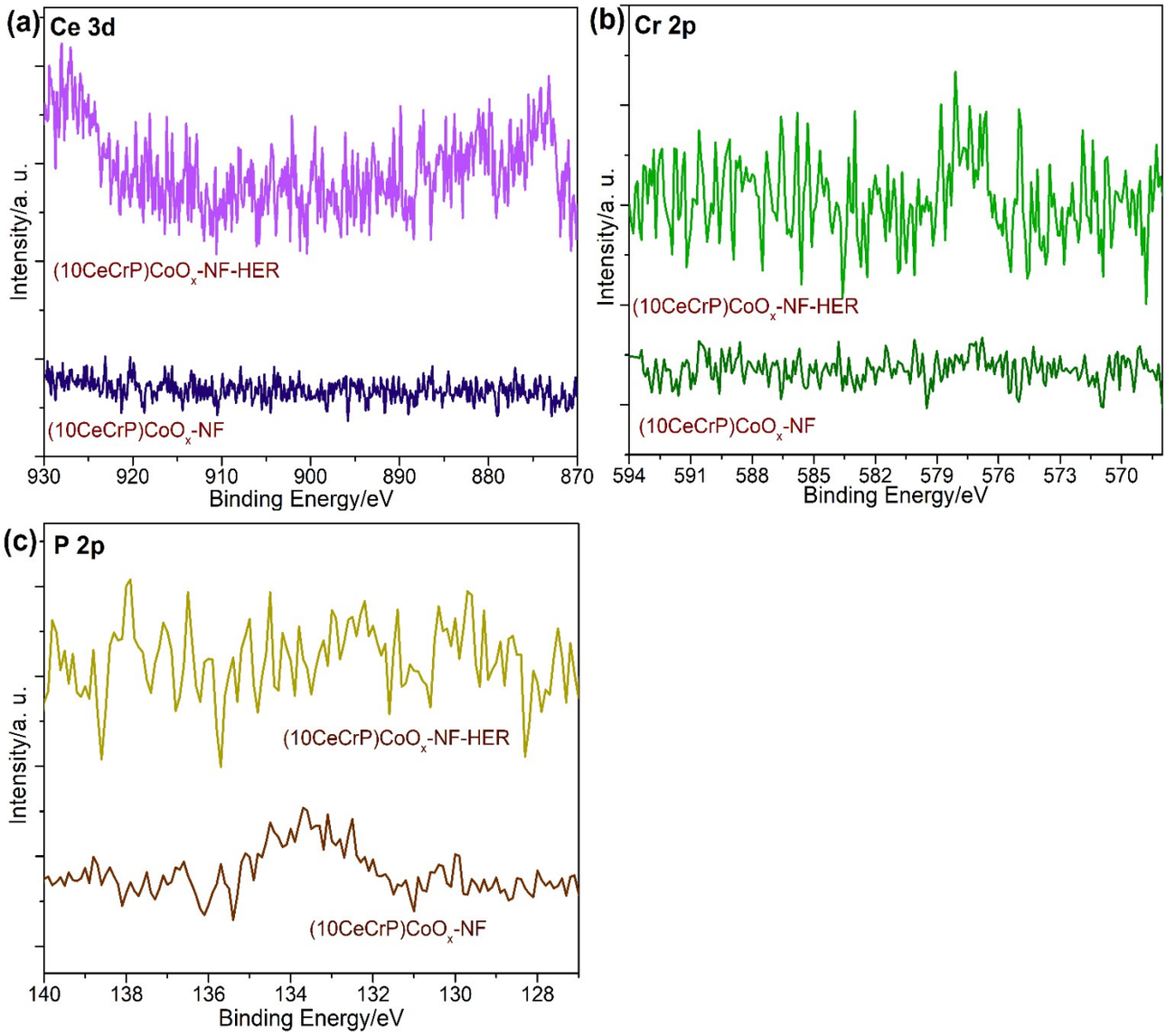


**Figure S14.** XPS spectra of (10CeCrP)$CoO_x$-NF and (10CeCrP)$CoO_x$-NF-HER. (a) Ce 3d; (b) Cr 2p and (c) P 2p.

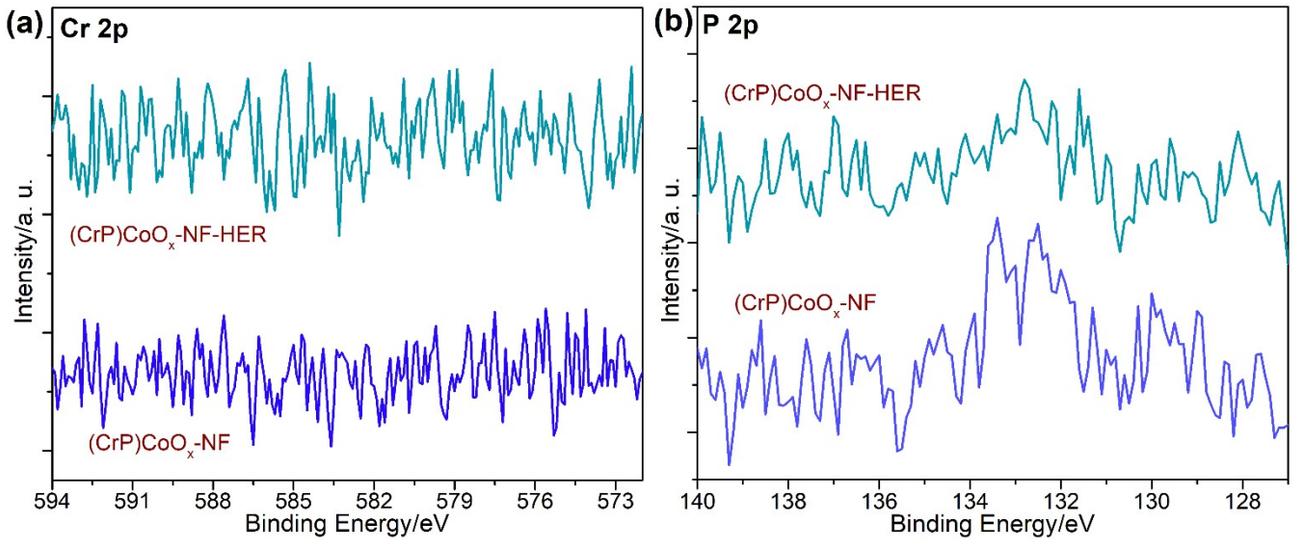


**Figure S15.** (a) Cr 2p and (b) P 2p XPS spectra of (CrP)$CoO_x$-NF and (CrP)$CoO_x$-NF-HER.

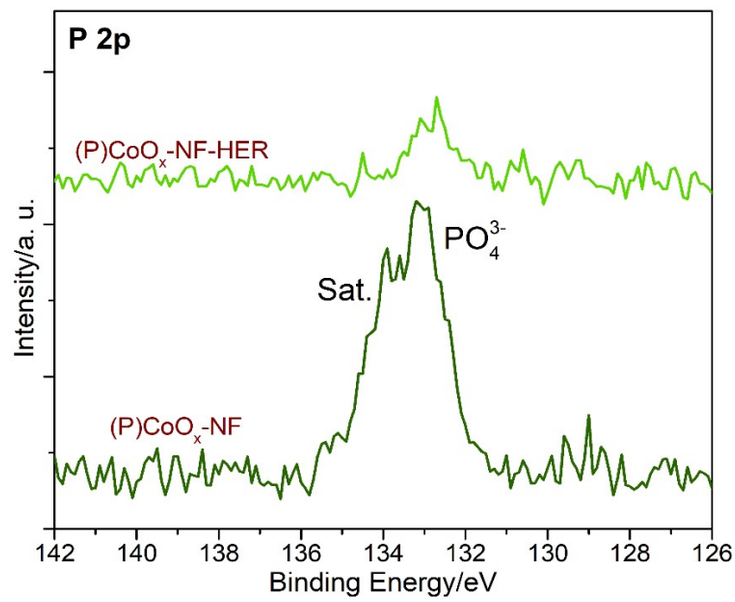


**Figure S16.** P 2p XPS spectra of (P)$CoO_x$-NF and (P)$CoO_x$-NF-HER.

The chemical states of Cr, Ce and P in the electrocatalysts were studied by XPS. We can see that for the XPS spectra of (10CeCrP)$CoO_x$-NF and (10CeCrP)$CoO_x$-NF-HER, no obvious Ce 3d, Cr 2p and P 2p characteristic peaks can be observed (Figure S14). Meanwhile, the XPS spectra of (CrP)$CoO_x$-NF and (CrP)$CoO_x$-NF-HER show no obvious characteristic peaks of Cr 2p and P 2p too (Figure S15). For the XPS spectrum of (P)$CoO_x$-NF, two characteristic peaks can be observed, represent $PO_4^{3-}$ and its satellite peak.[6, 7] Compared with (P)$CoO_x$-NF, those characteristic peaks of (P)$CoO_x$-NF-HER become weaker, suggesting the P element leaches out during HER (Figure S16). Those results suggest that the Ce, Cr and P plays negligible role in HER.

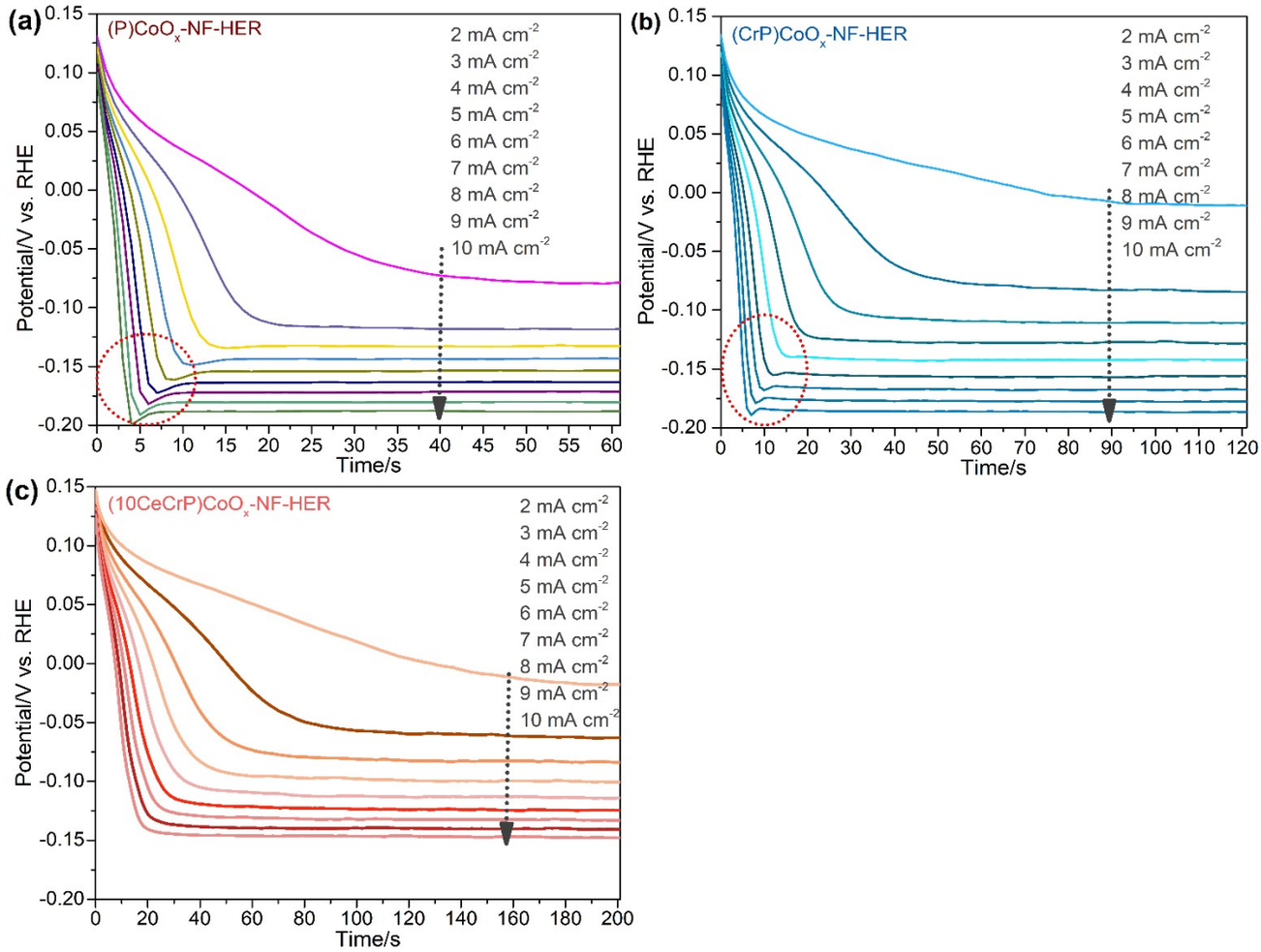


**Figure S17.** Potential-time dependent curves of (a) (P)$CoO_x$-NF-HER, (b) (CrP)$CoO_x$-NF-HER and (c) (10CeCrP)$CoO_x$-NF-HER measured at 2~10 mA $cm^{-2}$.

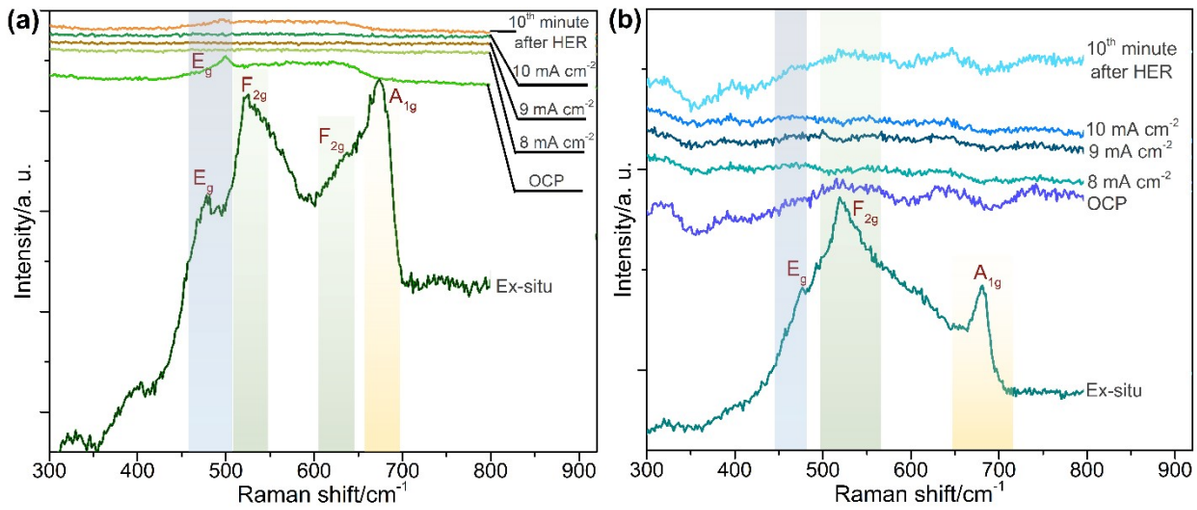


**Figure S18.** Raman spectra: (a) (P)$CoO_x$-NF-HER and (b) (CrP)$CoO_x$-NF-HER.

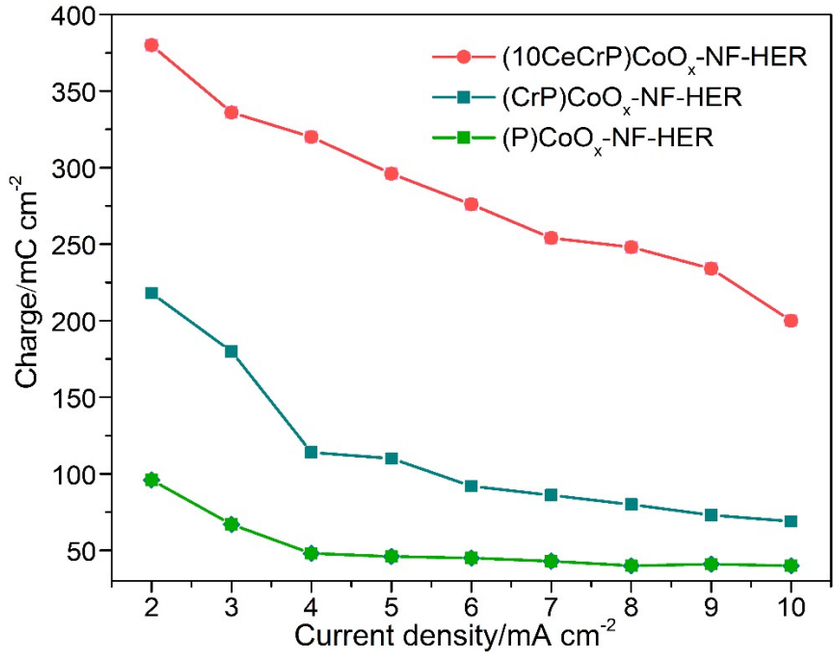


**Figure S19.** Plots of charge-current density for (10CeCrP)$CoO_x$-NF-HER, (CrP)$CoO_x$-NF-HER and (P)$CoO_x$-NF-HER.

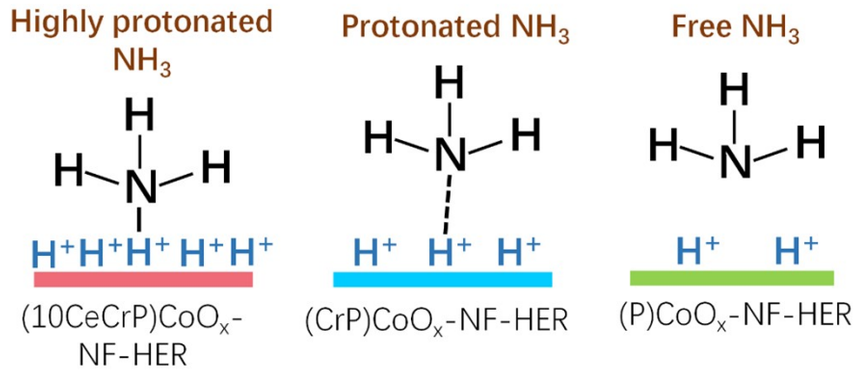


**Figure S20.** Scheme of different interactions between protons and probe molecule ($NH_3$) on (10CeCrP)$CoO_x$-NF-HER, (CrP)$CoO_x$-NF-HER and (P)$CoO_x$-NF-HER.

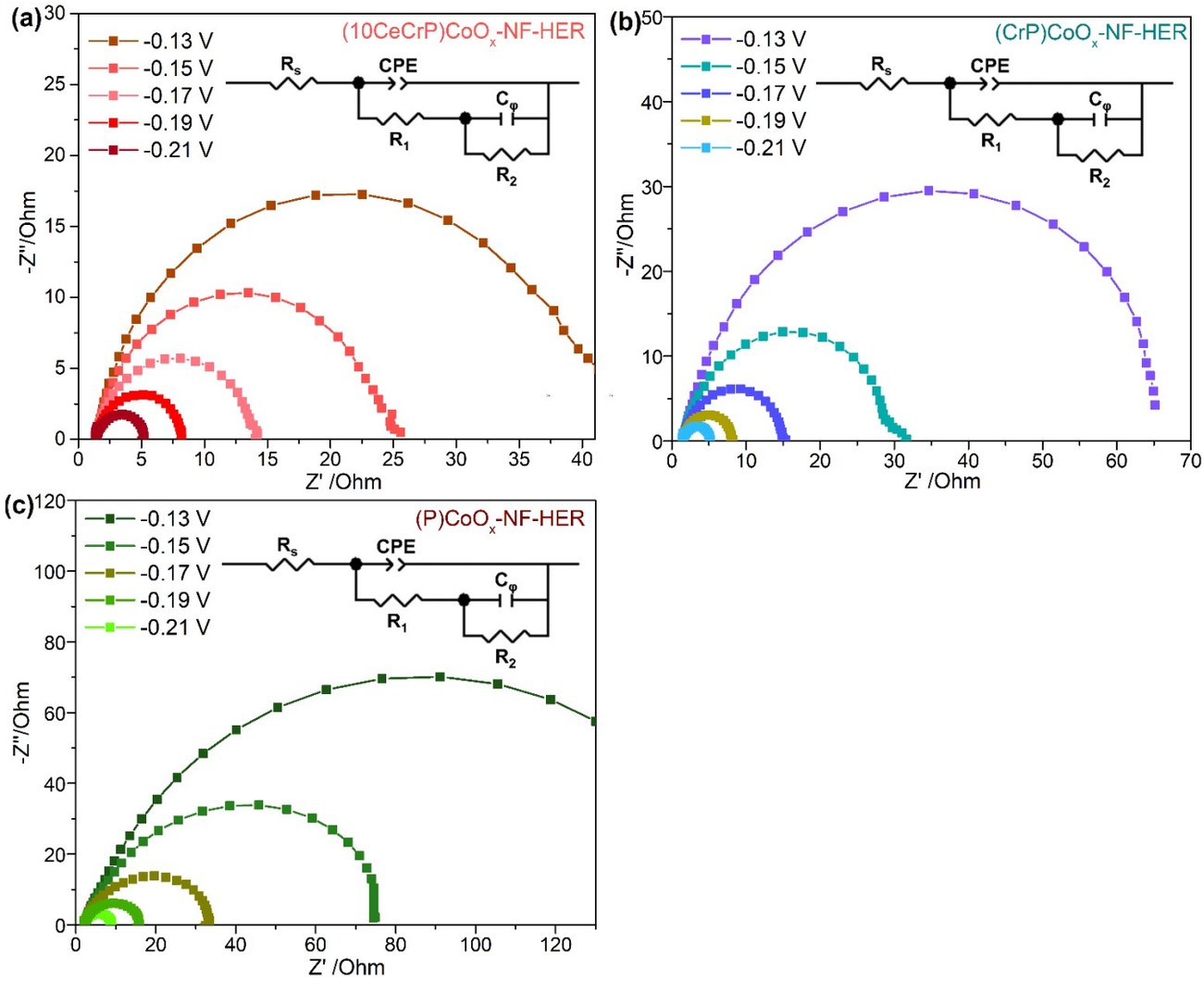


**Figure S21.** Nyquist plots of (a) (10CeCrP)$CoO_x$-NF-HER, (b) (CrP)$CoO_x$-NF-HER and (c) (P)$CoO_x$-NF-HER. Inset: the electronic circuit utilized to fit the curve.

**Table S5.** The fitted parameters of the EIS data of the (10CeCrP)$CoO_x$-NF-HER, (CrP)$CoO_x$-NF-HER and (P)$CoO_x$-NF-HER.

| Catalyst | Potential/V vs. RHE | $R_s/\Omega$ | $C_T/(F\ S^n)^{-1}$ | $C_p$ | $R_1/\Omega$ | $R_2/\Omega$ | $C_\varphi/F$ |
|---|---|---|---|---|---|---|---|
| (10CeCrP)$CoO_x$-NF-HER | -0.13 | 1.342 | 0.0189 | 0.8874 | 1.683 | 38.07 | 0.00532 |
| | -0.15 | 1.341 | 0.0172 | 0.8847 | 1.158 | 22.15 | 0.00552 |
| | -0.17 | 1.343 | 0.0150 | 0.9015 | 1.08 | 11.55 | 0.00640 |
| | -0.19 | 1.341 | 0.0134 | 0.8971 | 0.6728 | 6.299 | 0.00678 |
| | -0.21 | 1.353 | 0.0108 | 0.9308 | 0.6298 | 3.223 | 0.00811 |
| (CrP)$CoO_x$-NF-HER | -0.13 | 1.409 | 0.0131 | 0.8440 | 2.028 | 69.92 | 0.00267 |
| | -0.15 | 1.409 | 0.0107 | 0.8582 | 1.345 | 27.91 | 0.00306 |
| | -0.17 | 1.404 | 0.0088 | 0.8659 | 0.9108 | 12.95 | 0.00339 |
| | -0.19 | 1.409 | 0.00680 | 0.8825 | 0.5765 | 6.22 | 0.00377 |
| | -0.21 | 1.404 | 0.00448 | 0.9096 | 0.4051 | 3.379 | 0.00442 |
| (P)$CoO_x$-NF-HER | -0.13 | 2.032 | 0.00770 | 0.8368 | 54.68 | 122.6 | 0.000428 |
| | -0.15 | 2.038 | 0.00687 | 0.8542 | 36.39 | 44.69 | 0.00254 |
| | -0.17 | 2.035 | 0.00619 | 0.8663 | 16.26 | 16.38 | 0.00193 |
| | -0.19 | 2.003 | 0.00450 | 0.8513 | 1.009 | 13.2 | 0.00137 |
| | -0.21 | 1.991 | 0.00279 | 0.8754 | 0.5391 | 6.508 | 0.00189 |

Nyquist plots were simulated by a double-parallel equivalent circuit model. The first parallel components ($C_T$ and $R_1$) reflect the charge-transfer kinetics, in which $C_T$ is related to the double layer capacitance and $R_1$ represents catalytic charge-transfer resistance.[8-10]

## References


1. Y. Li, W. Qiu, F. Qin, H. Fang, V. G. Hadjiev, D. Litvinov and J. Bao, Identification of Cobalt Oxides with Raman Scattering and Fourier Transform Infrared Spectroscopy, *J. Phys. Chem. C*, 2016, **120**, 4511-4516.
2. B. Rivas-Murias and V. Salgueiriño, Thermodynamic CoO-$Co_3O_4$ crossover using Raman spectroscopy in magnetic octahedron-shaped nanocrystals, *J. Raman Spectrosc.*, 2017, **48**, 837-841.
3. J. Wang, R. Gao, D. Zhou, Z. Chen, Z. Wu, G. Schumacher, Z. Hu and X. Liu, Boosting the Electrocatalytic Activity of $Co_3O_4$ Nanosheets for a Li-$O_2$ Battery through Modulating Inner Oxygen Vacancy and Exterior $Co^{3+}/Co^{2+}$ Ratio, *ACS Catal.*, 2017, **7**, 6533-6541.
4. Y. Li, R. Li, D. Wang, H. Xu, X. Lu, L. Xiao, F. Meng, J. Zhang, M. An and P. Yang, Pulse electrodeposited CoFeNiP as a highly active and stable electrocatalyst for alkaline water electrolysis, *Sustainable Energy & Fuels*, 2021, **5**, 3172-3181.
5. Y. Ma, H. Wang, X. Lv, D. Xiong, H. Xie and Z. Zhang, Three-dimensional ordered mesoporous $Co_3O_4$/peroxymonosulfate triggered nanoconfined heterogeneous catalysis for rapid removal of ranitidine in aqueous solution, *Chem. Eng. J.*, 2022, **443**, 136495.
6. Y.-R. Liu, W.-H. Hu, X. Li, B. Dong, X. Shang, G.-Q. Han, Y.-M. Chai, Y.-Q. Liu and C.-G. Liu, One-pot synthesis of hierarchical $Ni_2P/MoS_2$ hybrid electrocatalysts with enhanced activity for hydrogen evolution reaction, *Appl. Surf. Sci.*, 2016, **383**, 276-282.
7. Y. Wang, Y. Jiao, H. Yan, G. Yang, C. Tian, A. Wu, Y. Liu and H. Fu, Vanadium-Incorporated CoP2 with Lattice

Expansion for Highly Efficient Acidic Overall Water Splitting, *Angew. Chem. Int. Ed.*, 2022, **61**, e202116233.

8. R. Šimpraga, G. Tremiliosi-Filho, S. Y. Qian and B. E. Conway, In situ determination of the 'real are factor' in $H_2$ evolution electrocatalysis at porous Ni-Fe composite electrodes, *J. Electroanal. Chem.*, 1997, **424** 141-151.
9. N. V. Krstajić, B. N. Grgur, N. S Mladenović, M. V. Vojnović and M. M. Jakšić, The determination of kinetics parameters of the hydrogen evolution on Ti-Ni alloys by ac impedance, *Electrochim. Acta*, 1997, **42**, 323-330.
10. A. Damian and S. Omanovic, Ni and NiMo hydrogen evolution electrocatalysts electrodeposited in a polyaniline matrix, *J. Power Sources*, 2006, **158**, 464-476.